

Low Temperature Synthesis of spinel-type $\text{Co}_x\text{Fe}_{3-x}\text{O}_4$ ($0 \leq x \leq 1.5$) Oxide and its Application for Oxygen Evolution Electrocatalysis in Alkaline Solution

Narendra Kumar Singh*, Manish Kumar Yadav, Reena Parihar and Indresh Kumar

Department of Chemistry, Faculty of Science, University of Lucknow, Lucknow-226007, India

*E-mail: nksbhu@yahoo.com, singh_narendra@lkouniv.ac.in,

Received: 15 February 2020 / Accepted: 17 April 2020 / Published: 10 June 2020

Spinel-type Fe_3O_4 and its Co-substituted products were synthesized at 80°C by a co-precipitation method and investigated for their electrocatalytic properties in the form of oxide film electrode on Ni-support towards oxygen evolution reaction (OER) in alkaline medium. X-ray diffraction study indicated the formation of almost pure spinel ferrite phase with some impurities, which is found basically in the case of $\text{Co}_{0.5}\text{Fe}_{2.5}\text{O}_4$ oxide. The formation of spinel ferrite was also confirmed by recording the IR spectra. The cyclic voltammogram was carried out in the potential region 0.0 – 0.7 V and shows a pair of redox peaks; one an anodic ($E_{\text{Pa}} = 524 \pm 36$) and corresponding cathodic ($E_{\text{Pc}} = 351 \pm 6$) peak prior to the onset of oxygen evolution reaction. The anodic polarization study showed that the substitution of Co for Fe in the Fe_3O_4 lattice strongly affects the electrocatalytic properties of the materials. The optimum improvement in the activity is being with 1.0 mol Co-substitution. At $E = 850$ mV vs Hg/HgO/1M KOH (25°C), the current density with CoFe_2O_4 ($j = 315.6$ mA cm^{-2}) oxide was about 13 time higher than Fe_3O_4 . The Tafel slope values also decreased from 68 mV decade⁻¹ to 44 mV decade⁻¹ with Co-substitution. The thermodynamic parameters have been calculated for the oxide electrode, CoFe_2O_4 , at different potentials. It appears that as the potential is increased, the electrochemical standard enthalpy of activation ($\Delta H_{\text{el}}^{\circ\#}$) of the oxide is decreased. SE-micrograph indicates that the substitution of Co for Fe decreases the crystallite size of the materials.

Keywords: Co-precipitation, spinel ferrites, XRD, oxygen evolution, thermodynamic parameters

1. INTRODUCTION

In the present era of fast-moving global development, energy is one of the most important issues. The conventional sources of energy like fossil fuels and oils deposits are limited and it is expected that these fossil fuels and oils will be exhausted by the mid of current century [1]. Also, the pollution caused by using these fuels is a giant problem in front of us. In this scenario, hydrogen can be a clean and

effective option and would be the fuel of the future. Production of hydrogen and oxygen gases at industrial scale by the electrolysis of alkaline water is a problematic task because high amount of electrical energy consume in the process due to hydrogen and oxygen overpotentials. Use of efficient electrocatalyst can reduce the overpotential values to the great extent and also prevent the electrode from early polarization. Various types of electrocatalysts like metals, metal alloys, metal oxides, metal mixed oxides etc. are being used. An electrocatalyst may be in the form of coating at any substrate or may be itself as an electrode. Transition metal mixed oxides with spinel and perovskite type structure are found to be very promising electrocatalytic materials for anodic evolution of oxygen and cathodic evolution of hydrogen. In the recent years, spinel type ferrite materials have been intensively explored because of their remarkable physical and chemical properties and broad practical applications in various fields like data storage systems, magnetic tapes & filters, medical diagnostics, drug delivery, transformer cores etc. These materials also extensively been used for decomposition of hydrogen peroxide [2,3], synthesis of ammonia [4], oxidation of butadiene [5] and for the synthesis of chlorine and chlorates [6]. Various synthetic methods have been developed for the preparation of these oxides like thermal decomposition [7,8], freeze drying [9], citrate precursor technique [10], coprecipitation [11], sol-gel [12,13], hydrothermal [14], etc.

The electrocatalytic properties of these materials depend on the various factors like preparation method, temperature, metal ion substitution and pH of the precursor solution. It has been observed that the earlier used high temperature preparation methods [9,15] produced the oxides with low specific surface area, high resistivity and hence low electrocatalytic activity. Aiming to improve the electrocatalytic activity to a reasonable high extent, some low temperature methods have been developed in past few decades, namely coprecipitation [16, 17], sol-gel [13,18,19]. Also, it has been found that optimum substitutions of certain metal cations in the oxide improve their catalytic activity towards oxygen reaction [19-24]. Singh et al [16, 23-27] synthesized a series of metal substituted binary and ternary ferros spinels at pH = 11 by adopting low temperature co-precipitation method and observed augmentation in the electrocatalytic properties of materials towards OER. In the preparation of each series, they used metal sulfates as starting materials. Very recently [28-33], we have studied the electrocatalytic properties for OER of some spinel ferrites obtained by novel low temperature routes and observed significant influence of preparation methods, precursors and metal ions substitution. Recently, Tao et al [34] prepared copper substituted ferrite by using another coprecipitation method to study its gas sensing properties. We adopted the same method [34] and produced Co-substituted spinel ferrites and studied their physicochemical and electrochemical properties for OER in alkaline medium. The results, so obtained, in study are described in this paper.

2. MATERIALS AND METHODS

Spinel type nano sized $\text{Co}_x\text{Fe}_{3-x}\text{O}_4$ ($0 \leq X \leq 1.5$) oxide materials were synthesized by using coprecipitation method [34]. Metal nitrate salts were used as cation precursors in each preparation. Analytical grade cobalt (II) nitrate hexahydrate [$\text{Co}(\text{NO}_3)_2 \cdot 6\text{H}_2\text{O}$], iron (III) nitrate nonahydrate [$\text{Fe}(\text{NO}_3)_3 \cdot 9\text{H}_2\text{O}$] and sodium hydroxide (NaOH) were used as starting materials. In a typical procedure,

a stoichiometric amount of metal nitrates was dissolved in 100 ml double distilled water and a 75 ml hot 4M NaOH solution was slowly added to get a precipitate. The precipitate was heated at 90°C for 2 hours and then filtered, washed several times with redistilled water and finally dried for overnight at 80°C to get the desired oxide material.

Materials, so obtained, were characterized physicochemically by using Powder X-Ray diffraction (XRD) (XPRT-PRO X-Ray diffractometer, Model: PW 3050/60) using Cu-K α ($\lambda = 1.54048 \text{ \AA}$) radiation source. Surface morphology of oxide powders was determined by scanning electron microscope (SEM, Model: LEO430). Spinel ferrite phase of the oxide materials was determined by FTIR spectroscopy (Thermoscientific, Nicole-6700). The spectra of each composition were recorded in the frequency range of 4000-400 cm^{-1} in the form of pellet with analytical grade KBr.

The electrocatalytic properties of prepared oxides was tested in the form electrode, which was prepared by coating over a pretreated nickel plate of approximate area 1.5 cm^2 using oxide slurry painting technique [35,36]. In this technique, a small amount of dried oxide was mixed with few drops of Triton X-100 in an agate pastel-mortar and mixed thoroughly to get a pasty mass. This paste was coated over one side of a pretreated Nickel plate using a fine brush. The coated plate was heated in an electrical muffle furnace (ASCO) at 380°C for 1.5h. For the better adherence of oxide film over the nickel plate, the plate was removed only when the furnace was attended the temperature below 80°C. If required second and third coating was also performed to get the desired loading in mg.cm^{-2} . Copper wire and silver paint were used to make electrical contact of plate by applying the technique as described in literature [36]. Both surfaces of the nickel plate were finally coated with a layer of Araldite epoxy adhesive except 0.5 cm^2 oxide coated area. This uncoated area was used for all types of electrochemical study of oxide material. Electrochemical analysis of film electrodes was performed in a conventional three electrode single compartment glass cell. Electrodes were connected to a Potentiostat/Galvanostat associated to a personal computer with corrosion and physical electrochemical study software (Gamry Reference 600 ZRA). A platinum foil having approximate area 2 cm^2 and Hg/HgO/1M KOH were used as counter and reference electrodes, respectively. The reference electrode was connected with the cell solution through a Luggin capillary (KCl/Agar-Agar salt bridge) to minimize the solution resistance (iR drop) between working and reference electrodes.

3. RESULT AND DISCUSSION

3.1 Physicochemical Study

3.1.1 Scanning Electron Micrograph (Sem)

The scanning electron micrographs of the oxide powders, recorded at the magnification of $\times 500$, are shown in the Fig. 1 (a-d). The morphology of oxide powders was observed to be almost same and found to be crystalline in nature. Co-substitution in the base oxide reduces the crystallite size and seems to be minimal for 1.0 mol cobalt substituted ferrite.

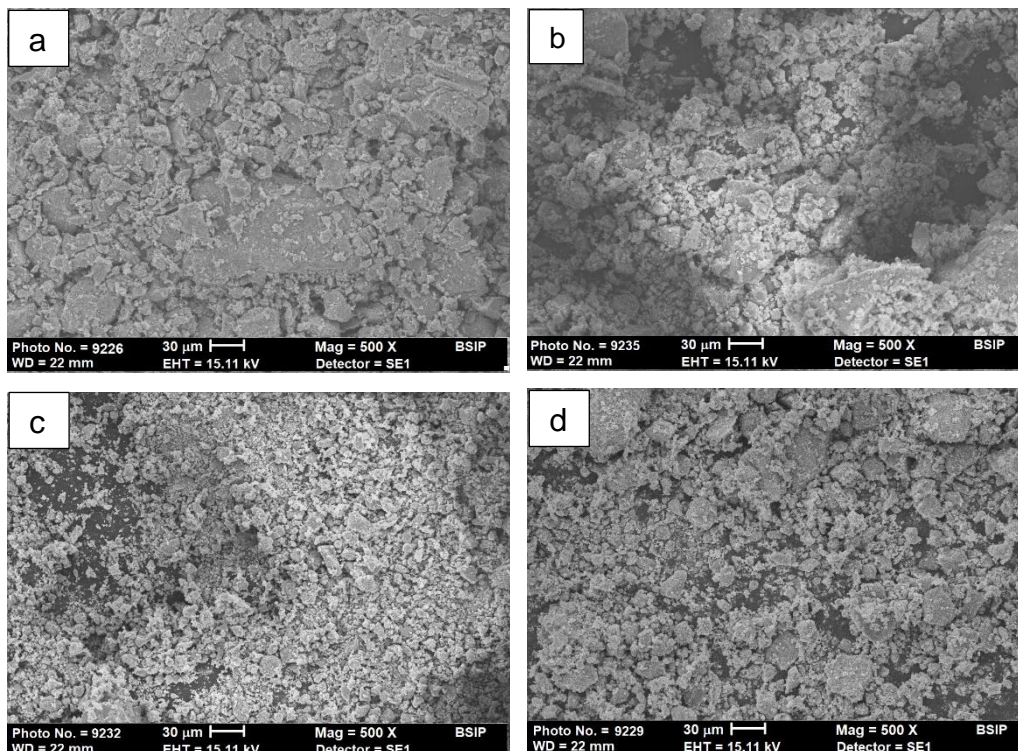


Figure 1. SE Micrograph of oxide powder heated at 80°C for 12 hrs at magnification $\times 500$. a: Fe_3O_4 ; b: $\text{Co}_{0.5}\text{Fe}_{2.5}\text{O}_4$; c: CoFe_2O_4 ; d: $\text{Co}_{1.5}\text{Fe}_{1.5}\text{O}_4$

3.1.2 Infrared Spectra (Ir)

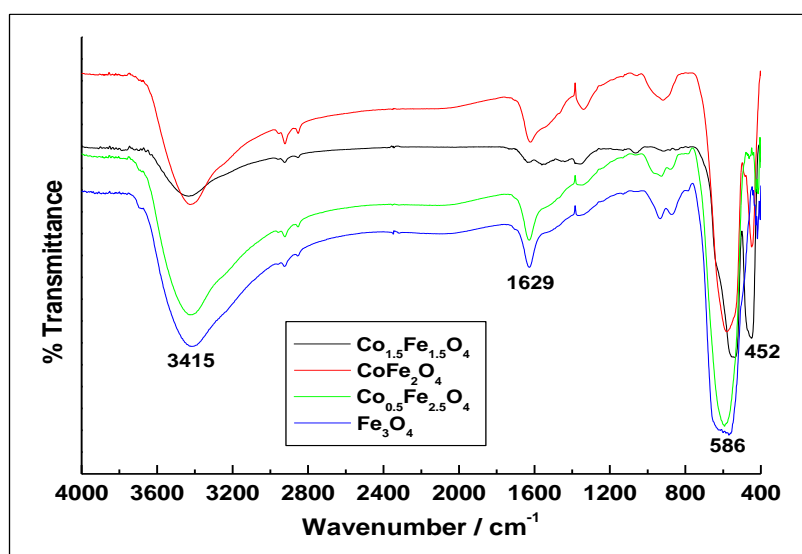


Figure 2. IR Spectra of the oxide powder synthesized at 80°C.

IR spectra of pure and cobalt substitutes ferrite oxide powders was recorded in the wave length region of 4000 to 400 cm^{-1} . The two characteristic strong peaks, obtained at 586 cm^{-1} and $\sim 456 \text{ cm}^{-1}$ correspond to the pure spinel ferrite [37, 38]. The broad peak at $\sim 3415 \text{ cm}^{-1}$ and poorly intense peak at $\sim 1629 \text{ cm}^{-1}$ indicated the O-H stretching vibrations interacting through H-bonds. The characteristics bands found with these materials are very much similar to that reported in literature [29, 31].

3.1.3 Powder X-Ray Diffraction (Xrd)

Fig. 3 represents the powder X-Ray diffraction pattern of the three representative oxides namely, $\text{Co}_{0.5}\text{Fe}_{2.5}\text{O}_4$, CoFe_2O_4 and $\text{Co}_{1.5}\text{Fe}_{1.5}\text{O}_4$, recorded in the scan window $2\theta = 20^\circ$ to 80° . With exception of $\text{Co}_{0.5}\text{Fe}_{2.5}\text{O}_4$, the X-ray diffraction patterns indicated the formation of almost pure spinel phase and best matched with JCPDS-ASTM file 22-1086. In the case of $\text{Co}_{0.5}\text{Fe}_{2.5}\text{O}_4$, some additional spectral lines of $\alpha\text{-Fe}_2\text{O}_3$ or $\alpha\text{-FeO(OH)}$ (JCPDS ASTM file 3-0249), Fe_2O_3 (JCPDS ASTM file 33-664) and $\delta\text{-Fe}_2\text{O}_3$ (JCPDS ASTM file) have been observed alongwith spinel phase. The average crystallite size was estimated by using Scherrer equation [39] and were found 17, 11 and 6 nm for $\text{Co}_{0.5}\text{Fe}_{2.5}\text{O}_4$, CoFe_2O_4 and $\text{Co}_{1.5}\text{Fe}_{1.5}\text{O}_4$ oxides, respectively.

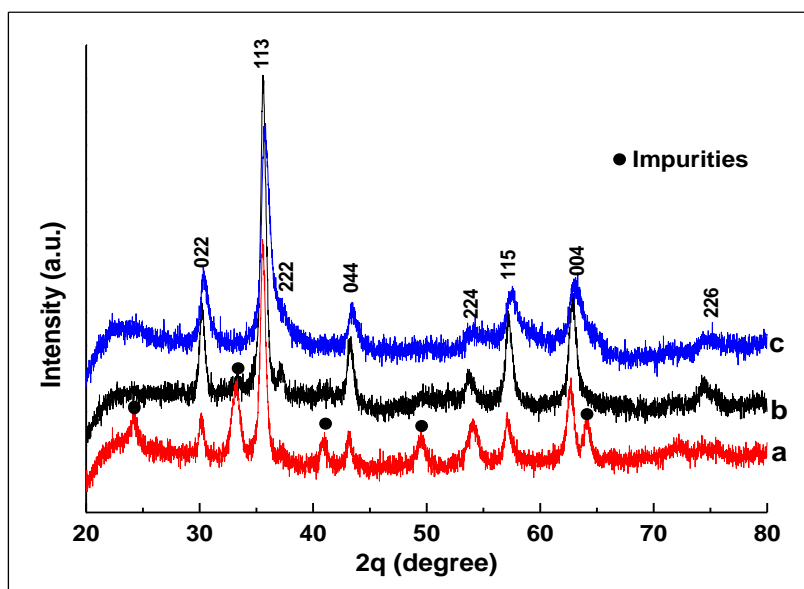


Figure 3. XRD powder patterns of oxide powder synthesized at 80 °C. a: $\text{Co}_{0.5}\text{Fe}_{2.5}\text{O}_4$, b: CoFe_2O_4 , c: $\text{Co}_{1.5}\text{Fe}_{1.5}\text{O}_4$

The strain and grain size for the oxide, $\text{Co}_{0.5}\text{Fe}_{2.5}\text{O}_4$, were also calculated with the help of Williamson-Hall plot [40,41]. For the purpose, values of $\beta\text{Cos}\theta/\lambda$ were plotted against $\epsilon\text{Sin}\theta/\lambda$, and represented in Fig. 4. The value of strain (ϵ) was calculated by measuring the slope of the straight line. The reciprocal of intercept at y-axis gives the value of crystallite size of the oxide powder. The estimated values of strain and grain size were found to be 0.0008 and 21 nm, respectively. The very low value of

strain indicated the approach of synthesized oxide towards homogeneity. The value of grain size for $\text{Co}_{0.5}\text{Fe}_{2.5}\text{O}_4$ oxide as calculated by Williamson-Hall plot and Scherrer's equation was observed to be almost similar.

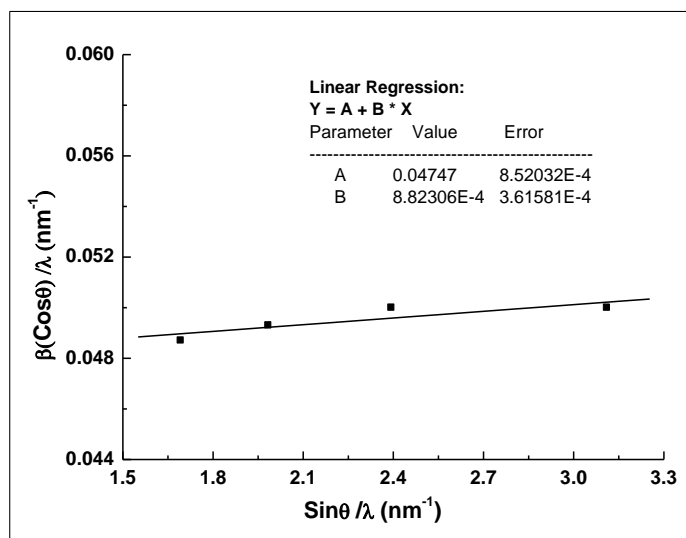


Figure 4. Williamson-Hall plot for $\text{Co}_{0.5}\text{Fe}_{2.5}\text{O}_4$ oxide.

3.2. Electrochemical Study

3.2.1 Cyclic Voltammetry (Cv)

The redox behavior of oxide film electrodes was determined by recording cyclic voltammogram in 1M KOH at 25 °C at the scan rate of 20 mV sec⁻¹ in potential window 0.0 to 0.7 V vs Hg/HgO/KOH(1M) ($E^\circ = 0.098$ V Vs. NHE). The recorded voltammograms as shown in Fig. 5 exhibited a single anodic ($E_{Pa} = 524 \pm 36$) and single cathodic ($E_{Pc} = 351 \pm 6$) peak prior to the onset of oxygen evolution reaction. The observed cathodic and anodic peak potentials are very much equivalent to the redox potential of pure Ni [16]. Such redox peaks were supposed to be originated from the substrate (Ni support) due to the contact with electrolyte [42] through pores, cracks, intercrystalline gaps formed in the catalytic film during experiment. Also, the oxide synthesized at low temperature are hydrophilic in nature and they undergo rapid hydration in aqueous solution resulting the wetting the whole film thickness [16] without affecting the stability of the catalytic overlayer. The estimated values of anodic (E_{Pa}) and cathodic (E_{Pc}) peak potentials, peak separation potential ($\Delta E_p = E_{Pa} - E_{Pc}$) and formal redox potential ($E^\circ = (E_{Pa} - E_{Pc})/2$) for surface redox reaction are given in the Table 1.

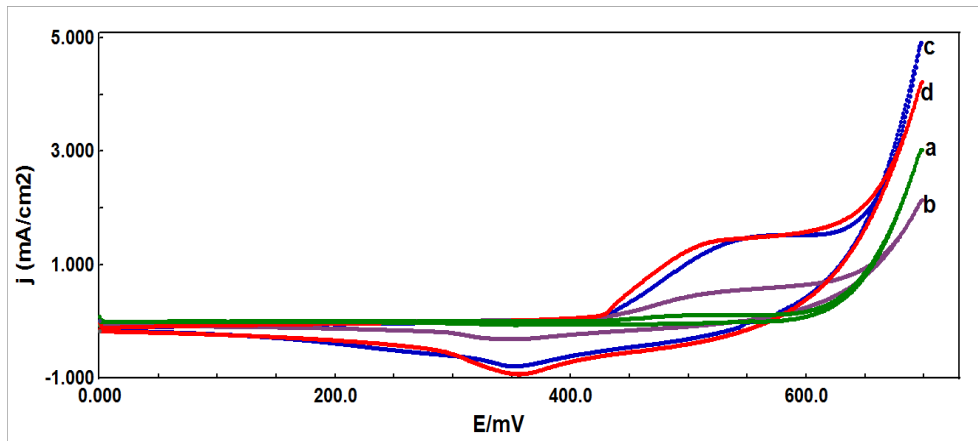


Figure 5. Cyclic voltammograms of pure and Co-substituted ferrite film electrode on Ni in 1M KOH at 25°C (scan rate = 20 mV sec⁻¹); a: Fe₃O₄, b: Co_{1.5}Fe_{1.5}O₄, c: CoFe₂O₄, d: Co_{0.5}Fe_{2.5}O₄.

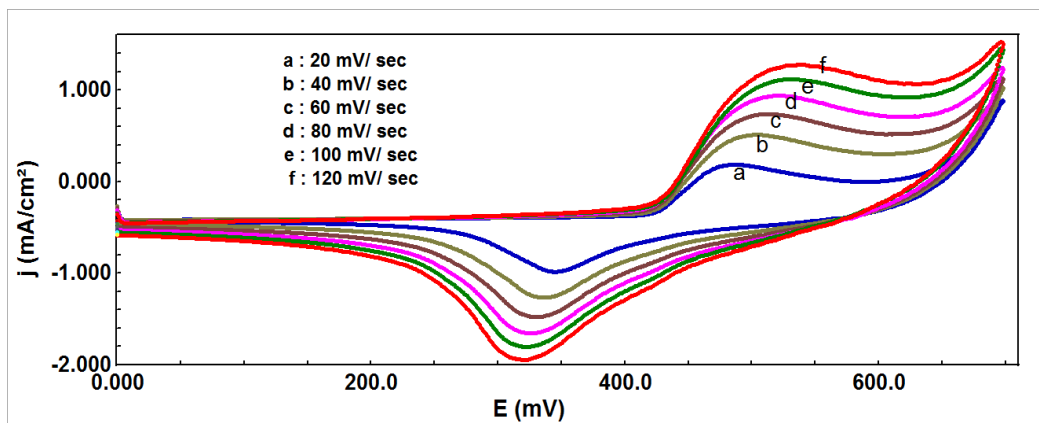


Figure 6. Cyclic voltammograms of the Fe₃O₄ film on Ni at different scan rates in 1M KOH (25°C).

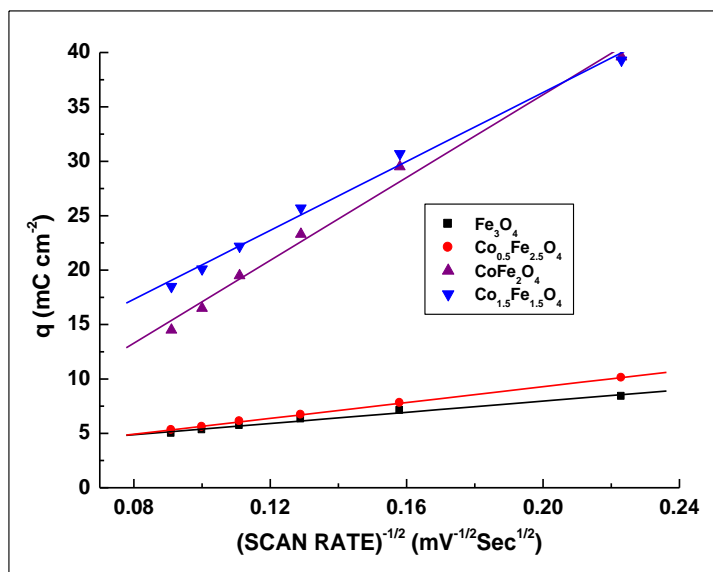


Figure 7. Plot of voltammetric charge (q) vs. (scan rate)^{-1/2} for the oxide electrode in 1M KOH (25°C).

To evaluate the effect of scan rate at the nature of cyclic voltammograms, the CV curves were recorded at varying scan rates in the range from 20 to 120 mV sec^{-1} under similar experimental conditions with each oxide film electrode. A representative set of voltammogram for Fe_3O_4 oxide film electrode is shown in the Fig. 6. The nature of voltammogram was found to be similar at each scan rate. However, a shift in the value of anodic and cathodic peak potential towards higher and lower potential sides, respectively, was observed with the increase of scan rate from 20 to 120 mV sec^{-1} . The observed shifting of cathodic and anodic peaks in either side with increase in scan rate indicates that the redox process is quasireversible. The estimated shift in anodic peak was 52-96 mV in positive direction whereas 24-27 mV in negative direction for cathodic peak. Such type shifting in the anodic and cathodic peak potential has also been observed with other spinel ferrites [29-33] obtained by different synthetic routes. The plots of voltammetric charge (q) vs. $(\text{scan rate})^{-1/2}$ were also constructed for each oxide electrode and shown in the Fig. 7. The straight line, as obtained in Figure 7, indicates that the surface redox process is diffusion controlled. The voltammetric charge was estimated by integrating the CV curve upto the potential just prior to the oxygen evolution reaction at each scan rate. It has been observed that values of voltammetry charge decrease with the increase of scan rate.

Table 1. Values of the Cyclic Voltammetric parameters of $\text{Ni}/\text{Co}_x\text{Fe}_{3-x}\text{O}_4$ ($0 \leq X \leq 1.5$) in 1 M KOH at 25 °C (scan rate = 20 mV sec^{-1})

Electrode	E_{Pa} /mV	E_{Pc} /mV	$\Delta E_P = (E_{Pa} - E_{Pc})$ /mV	$E^{\circ} = (E_{Pa} + E_{Pc})/2$ /mV	$ j_{Pa} $ /mA cm^{-2}	$ j_{Pc} $ /mA cm^{-2}	$\frac{ j_{Pa} }{ j_{Pc} }$	q /mC cm^{-2}
Fe_3O_4	487	345	142	416	0.6	0.4	1.5	8.4
$\text{Co}_{0.5}\text{Fe}_{2.5}\text{O}_4$	522	352	170	437	0.8	0.5	1.8	10.1
CoFe_2O_4	560	353	207	456	3.0	1.6	1.9	39.6
$\text{Co}_{1.5}\text{Fe}_{1.5}\text{O}_4$	527	356	171	442	2.9	1.9	1.5	39.3

3.2.2 Electrocatalytic Activity

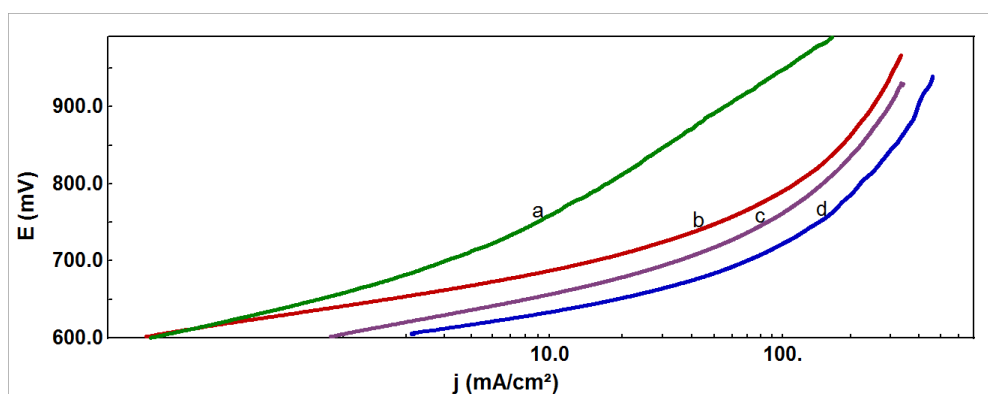


Figure 8. Anodic polarization curve for the oxide film electrode on Ni in 1MKOH at 25°C (scan rate: 0.2 mVsec^{-1}) a: Fe_3O_4 b: $\text{Co}_{0.5}\text{Fe}_{2.5}\text{O}_4$, c: $\text{Co}_{1.5}\text{Fe}_{1.5}\text{O}_4$, d: CoFe_2O_4 .

In order to determine and compare the electrocatalytic activity of oxide film electrodes towards oxygen evolution reaction (OER) in alkaline medium iR compensated anodic polarization curves (E vs. log j) were recorded in 1M KOH at 25°C, at slow scan rate of 0.2 mV sec⁻¹. The polarization curves, so obtained, with each oxide film electrodes are shown in Fig. 8.

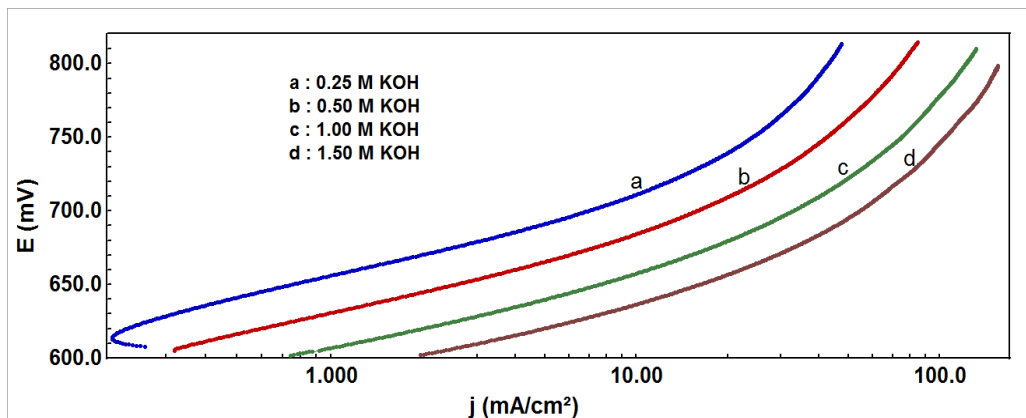


Figure 9. Anodic polarization curve for the CoFe₂O₄ film electrode on Ni at varying KOH concentrations ($\mu = 1.5$) at 25°C.

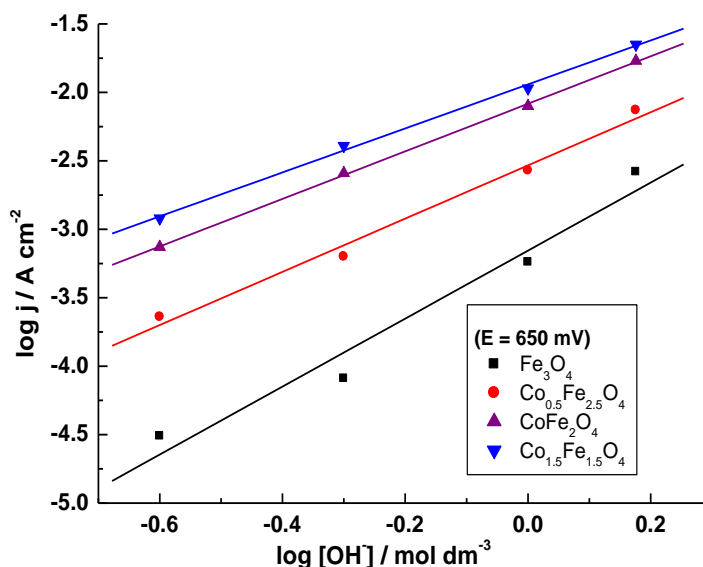


Figure 10. Plot of log j vs. log [OH⁻] for Co_xFe_{3-x}O₄ (0 ≤ x ≤ 1.5) film electrode on Ni at 25°C.

The nature of the polarization curve was observed to be similar with each oxide film electrode regardless of cobalt content. The values of Tafel slope (b), and electrocatalytic activity in terms of current density at a fixed potential as well as in terms of potential at a fixed current density were estimated from the polarization curve and given in the Table 2. It has been found that the substitution of cobalt in base

oxide reduces the values of Tafel slope and found minimum for 0.5 mol Co-substituted oxide film electrode. From table 2, it is observed that the substitution of Co for Fe in the Fe_3O_4 lattice increased the electrocatalytic activity greatly and the value was found to be highest with CoFe_2O_4 ($j_a = 315.6 \text{ mA cm}^{-2}$ at 850 mV). At a certain potential of 850 mV, the electrocatalytic activity of the oxide electrode towards OER follows the order:

CoFe_2O_4 ($j_a = 315.6 \text{ mA cm}^{-2}$) > $\text{Co}_{1.5}\text{Fe}_{1.5}\text{O}_4$ ($j_a = 219.2 \text{ mA cm}^{-2}$) > $\text{Co}_{0.5}\text{Fe}_{2.5}\text{O}_4$ ($j_a = 183.5 \text{ mA cm}^{-2}$) > Fe_3O_4 ($j_a = 60.25 \text{ mA cm}^{-2}$)

The reaction order for OER was determined by recording the anodic polarization curve in varying hydroxide ion concentration (0.25 to 1.5M) at 25°C. The ionic strength of the electrolytic solution was maintained by using inert electrolyte (KNO_3). Representative curve, so obtained, for CoFe_2O_4 oxide film electrode is shown in Fig. 9.

From the data of the polarization curve, a plot of $\log j$ vs. $\log [\text{OH}^-]$ (Fig. 10) was constructed at a certain applied potential for each film electrode. Order of reaction was determined by measuring the slope of the straight line and given in the Table 3.

Table 2. Electrode kinetic parameters for oxygen evolution reaction on pure and Co-substituted ferrite electrodes in 1 M KOH at 25°C

Electrode	Tafel slope /mVd ⁻¹	Order (p)	E/mV at j (mA cm ⁻²)		j (mA cm ⁻²) at E/mV		
			10	100	650	750	850
Fe_3O_4	68	2.4	787	965	0.6	5.9	23.7
$\text{Co}_{0.5}\text{Fe}_{2.5}\text{O}_4$	44	1.9	689	790	1.8	52.5	183.5
CoFe_2O_4	47	1.7	635	722	18.1	144.9	315.6
$\text{Co}_{1.5}\text{Fe}_{1.5}\text{O}_4$	57	1.6	660	762	7.2	85.9	219.2

It is noteworthy that the most active, CoFe_2O_4 , oxide electrode reported in this study has been found to electrocatalytic more beneficial than those of other spinel ferrite electrodes reported in literature. For example, Iwakura et al. [7,8] observed overpotential (η_{O_2}) 440 and 580 mV at current density 10 mA cm^{-2} in 1 M KOH at 25 °C. Mendonca et al. [43] and Godinho et al. [44] prepared $\text{CoFe}_{1.7}\text{Ni}_{0.3}\text{O}_4$ oxide film electrodes on Fe-support by using ceramic and solid state reaction methods, respectively. A current density, $j = 1.0 \text{ mA cm}^{-2}$, was reported at overpotential $\eta_{\text{O}_2} = 430 \text{ mV}$ for the oxide electrode obtained by ceramic method. Godinho et al. found Tafel slope of $63 \text{ mV decade}^{-1}$ with the exchange current density $j_o = 1.50 \times 10^{-10} \text{ A cm}^{-2}$ for the similar oxide. Similarly, Orehotzky et al. [9] observed oxygen overpotential, $\eta_{\text{O}_2} = 340 \text{ mV}$ at current density 10 mA cm^{-2} in 30 wt% for NiFe_2O_4 . Table 3 represents a list of electrocatalytic data of some spinel oxides synthesized by other low temperature methods. From the table, it is observed that in some cases, the electrocatalytic activity of the oxides conveyed in the present study is found to be better. However, in the case of others, they show

lower activity. With some exceptions, the Tafel slope of the oxide electrodes is very similar to those reported by other researchers.

Table 3. Comparison with reported spinel oxides for oxygen evolution reaction in 1 M KOH

Electrocatalysts	Tafel Slope (mV/decade)	E /mV (vs Hg/HgO/1M KOH) at $j = 100 \text{ mA cm}^{-2}$	Preparation method	Ref.
Ni/MnFe ₂ O ₄	36-42	641	COP	[16]
Ni/CoFe _{1.2} Cr _{0.8} O ₄	40	615	COP	[23]
Ni/Co _{1.5} Fe _{1.5} O ₄	46	693	COP	[24]
Ni/Co _{1.0} Mn _{0.5} Fe _{1.5} O ₄	55	646	COP	[24]
Ni/Ni _{0.5} Fe _{2.5} O ₄	42	674	COP	[26]
Ni/CuFeCrO ₄	50	728	COP	[25]
Ni/MMoO ₄ (M = Fe, Co & Ni)	37-44	658-685	Thermal Decomposition	[27]
Ni/Co _{1.5} Fe _{1.5} O ₄	44	828	NH ₄ OH Sol-gel Auto combustion	[28]
Ni/Ni _{0.5} Fe _{2.5} O ₄	102	865	Egg-white sol-gel	[29]
Ni/CoFe ₂ O ₄	49	806	Glycine sol-gel	[30]
Ni/Mn _{0.5} Fe _{2.5} O ₄	52	765	Egg-white sol-gel	[31]
Ni/Co _{1.25} Ni _{0.25} Fe _{1.5} O ₄	55	792	NH ₄ OH COP	[32]
Ni/Ni _{0.5} Fe _{2.5} O ₄	72	886	NH ₄ OH COP	[33]
Pt/CoFeCrO ₄	51	675	COP	[45]
Ni/NiFe ₂ O ₄	42	$j = 18.7 \text{ mA cm}^{-2}$ at 750 mV	Hydrothermal	[46]
Ni/NiFe _{1.5} V _{0.5} O ₄	40	$j = 122.0 \text{ mA cm}^{-2}$ at 700 mV	COP	[47]
Ni/NiMoO ₄	70	790	Precipitation	[48]
Ni/CoMoO ₄	60	731	Precipitation	[49]
Ni/CoFe₂O₄	47	722	COP	Present work

3.2.3 Thermodynamic Study

To explore the effect of temperature variation and to estimate the values of thermodynamic parameters, such as standard electrochemical energy of activation ($\Delta H_{el}^{0\ddagger}$), standard enthalpy of activation ($\Delta H^{0\ddagger}$) and standard entropy of activation ($\Delta S^{0\ddagger}$), anodic polarization curves were recorded at different temperatures in electrolytic solution from 20°C to 50°C in 1M KOH. During the experiment,

the temperature of reference electrode was kept constant at 25°C. The representative polarization curve for most active oxide film electrode (CoFe₂O₄) is shown in the Fig. 11.

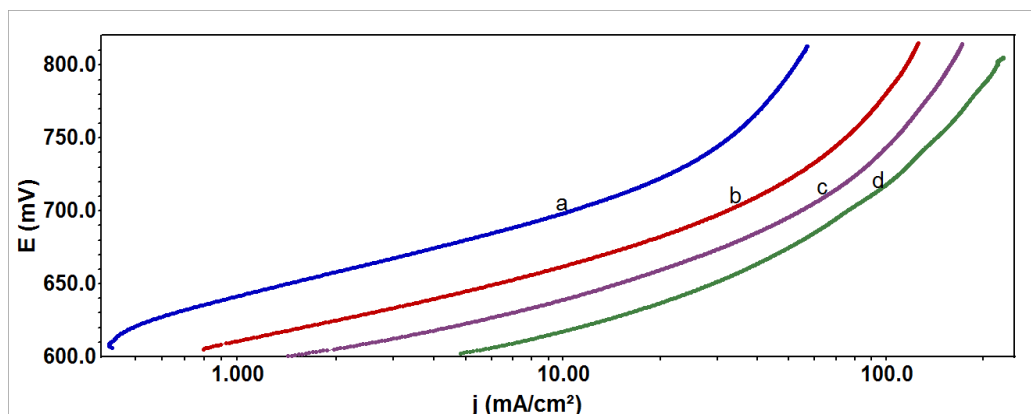


Figure 11. Anodic polarization curve for the CoFe₂O₄ film electrode on Ni at different temperatures in 1 M KOH; a: 20 °C; b: 30 °C; c: 40 °C; d: 50 °C.

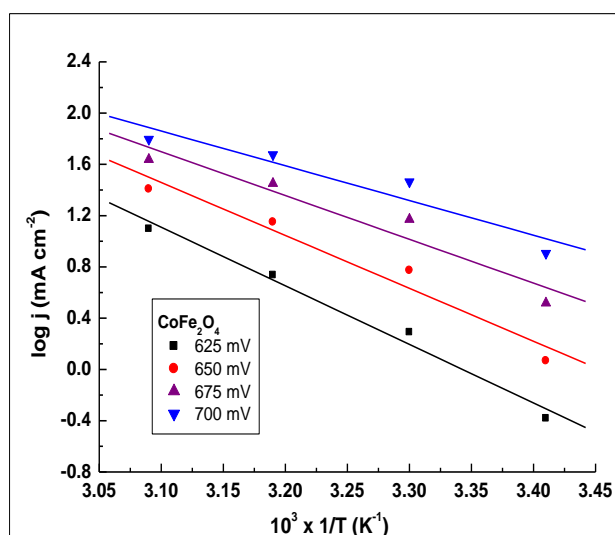


Figure 12. The Arrhenius plot at different constant applied potentials for CoFe₂O₄ in 1M KOH.

These curves were furnishing the values of current densities at different temperatures and by using this data, Arrhenius plot (log j vs. 1/T), was constructed at a various applied potential (Fig. 12). The slope of the straight line gives the value of $\Delta H_{el}^{o\#}$. Values of standard enthalpy of activation ($\Delta H^{o\#}$) and standard entropy of activation ($\Delta S^{o\#}$) were estimated by applying following relations (1) and (2) [50];

$$\Delta H_{el}^{o\#} = \Delta H^{o\#} - \alpha F \eta \quad \dots\dots\dots (1)$$

Where, α is the transfer coefficient equal to $2.303RT/bF$. The Tafel slope (b) is calculated from the polarization curves obtained at different temperatures. and R, F and T are the gas constant, Faraday constant and absolute temperature, respectively. η is the overpotential.

$$\Delta S^{\circ\ddagger} = 2.3R \left[\log j + \frac{\Delta H_{el}^{\circ\ddagger}}{2.3RT} - \log (n\omega F\omega C_{OH^-}) \right] \dots\dots(2)$$

Where, ω ($= k_B T/h$) is the frequency term and $n = 2$, k_B and h are the Boltzmann constant and Plank's constant, respectively. The calculated values of thermodynamic parameters are listed in the Table 4. It has been observed that the value of standard electrochemical energy of activation ($\Delta H_{el}^{\circ\ddagger}$) decreases with increase in applied potential. The reduction in $\Delta H_{el}^{\circ\ddagger}$ is also expected as per relation (1) and reported by us earlier [31, 51].

Table 4. Thermodynamic parameters for O₂ evolution on Ni/ CoFe₂O₄ in 1M KOH

E / mV	$\Delta H_{el}^{\circ\ddagger}$ (KJ mol ⁻¹)	$\Delta S^{\circ\ddagger}$ (J deg ⁻¹ mol ⁻¹)	$\Delta H^{\circ\ddagger}$ (KJ mol ⁻¹)
650	76.5	66.4	119.2
675	58.5	121.1	104.2
700	41.2	174.9	90.1

4. CONCLUSIONS

X-ray study indicates that the co-precipitation method produced oxide with some impurities basically in the case of Co_{0.5}Fe_{2.5}O₄. Substitution of Co in the base oxide (Fe₃O₄) influenced the electrocatalytic activity of the materials. The electrocatalytic activity of most active oxide film electrode (CoFe₂O₄) was found to be about 13 times more than base oxide. It produced current density, $j = 315.6$ mA cm⁻² at potential 850 mV in 1 M KOH at 25°C. A pair of redox peaks was observed in the cyclic voltammogram of each oxide electrode.

ACKNOWLEDGEMENTS

Authors are thankful to the department of Chemistry, University of Lucknow, Lucknow (INDIA) for providing essential infrastructures to carry out the experiments. Department of Science and Technology (DST), New Delhi is gratefully acknowledged for the financial support as Fast Track Scheme for Young Scientist (No.: SR/FT/CS-044/2009).

References

1. T. Abe, M. Kaneko, *Progress in Polymer Science*, 28 (2003)1441.
2. P. Lahari, S. K. Sengupta, *J. Chem. Soc. Faraday Trans.*, 91 (1995) 3489.
3. H. M. Kota, T. Katan, M. Chin, F. J. Schoenweis, *Nature*, 203 (1964) 1281.
4. R. R. Rajaram, P. A. Sermon, *J. Chem. Soc. Faraday Trans.*, 81 (1985) 2577.
5. H. K. Harold, C. K. Mayfair, *Adv. Catal.*, 33 (1985) 159.
6. S. Trasatti, G. Lodi, In: *Electrodes of conductive metallic oxides*, part B, ed. S. Trasatti Elsevier, Amsterdam, 1981.
7. C. Iwakura, M. Nishioka, H. Tamura, *Nippon Kagaku Kaishi*, 7 (1982) 1136.
8. C. Iwakura, M. Nishioka, H. Tamura, *Denki Kagaku*, 49 (1981) 355.
9. J. Orehotsky, H. Huang, C. R. Davidson, S, Srinivasan, *Journal of Electroanalytical Chemistry and Interfacial Electrochemistry*, 95 (1979) 233.

10. S. Prasad, N. S. Gajbhiye, *J. Alloys Compd.*, 265 (1998) 87.
11. J. M. Yang, W. J. Tsuo, F. S. Yen, *J. Solid State Chem.*, 145 (1999) 50.
12. D. H. Chen, X. R. He, *Mater Res Bull*, 36 (2001) 1369.
13. S. Maensiri, C. Masingboon, B. Boonchomb, *Scripta Materialia*, 56 (2007) 797.
14. J. Zhou, J. Ma, C. Sun, L. Xie, Z. Zhao, H. Tian, Y. Wang, J. Tao, X. Zhu, *J. Am. Ceram. Soc.*, 88 (2005) 3535.
15. I. Nikolov, R. Darkaou, E. Zhechevo, R. Stayanova, N. Dimitrov, T. Vitanov, *J. Electroanal. Chem.*, 429 (1997) 157.
16. N. K. Singh, S. K. Tiwari, K. L. Anitha, R. N. Singh, *J. Chem. Soc. Faraday Trans.*, 92(13) (1996) 2397.
17. G.-H. Li, L.-Z. Dai, D.-S. Lu, S.-Y. Peng, *J. Solid State Chemistry*, 89 (1990) 167.
18. M. El Baydi, G. Poillerat, J.-L. Rehspringer, J.-L. Gautier, J.-F. Koenig, P. Chartier, *J. Solid State Chem*, 109 (1994) 281.
19. J. L. Martin de Vidales, O. García-Martínez, E. Vila, R. M. Rojas, M. J. Torralvo, *Mat. Res. Bull.*, 28 (1993) 1135.
20. F. Svegli, B. Orel, I. Grabec-Svegli, V. Kaucic, *Electrochim. Acta.*, 45 (2000) 4359.
21. E. Rios, P. Chartier, J.-L. Gautier, *Solid State Sci.*, 1 (1999) 267.
22. P. D. Allen, N. A. Hampson, G. J. Bignold, *J. Electroanal. Chem.*, 99 (1979) 299.
23. R. N. Singh, N. K. Singh, J. P. Singh, *Electrochim. Acta*, 47 (2002) 3873.
24. J. P. Singh, N. K. Singh, R. N. Singh, *Int. J. Hydrogen Energy*, 24 (1999) 433.
25. R. N. Singh, J. P. Singh, B. Lal, A. Singh, *Int. J. Hydrogen Energy*, 32 (2007), 11.
26. N. K. Singh, R. N. Singh, *Ind. J. Chem.*, 38A (1999) 491.
27. R. N. Singh, J. P. Singh, A. Singh, *Int. J. Hydrogen Energy*, 33 (2008) 4260.
28. R. Yadav, M. K. Yadav, N. K. Singh, *Int. J. Electrochem. Sci.*, 8 (2013) 6321.
29. R. Yadav, Jhasaketan, N. K. Singh, *Int. J. Electrochem. Sci.*, 10 (2015) 9297.
30. R. Yadav, N. K. Singh, *Ind. J. Chem.*, 54A (2015) 1221.
31. N. K. Singh, R. Yadav, M. K. Yadav, *J. New Mat. Electrochem. System*, 19 (2016) 209.
32. N. K. Singh, Ritu Yadav, M. K. Yadav, Carlos Fernandez, *J. New Mat. Electrochem. Systems*, 20 (2017) 115.
33. R. Yadav, N. K. Singh, *Ind. J. Chemical Technol.*, 25 (2018) 189.
34. S. Tao, F. Gao, X. Liu, O. T. Sorensen, *Mater. Sci. Engg. B*, 77 (2000) 172.
35. R. N. Singh, S. K. Tiwari, S. P. Singh, N. K. Singh, *J. Chem. Soc. Faraday Trans.*, 92(14) (1996) 2593.
36. S. K. Tiwari, P. Chartier, R. N. Singh, *J. Electrochem. Soc.*, 142(1) (1995) 148.
37. N. Okasha, *Material Chem. and Phys.*, 84 (2004) 63.
38. B. Gillot, V. Nivoix, E. Kester, O. Nusillord, C. Villate, Ph. Tailhades, A. Sousset, *Mater. Chem. Phys.*, 48 (1997) 111.
39. N. Fradette, B. Marsan, *J. Electrochem. Soc.*, 145 (1998) 2320.
40. R. Kripal, A. K. Gupta, R. K. Srivastava, S. K. Mishra, *Spectrochimica Acta Part A: Molecular and biomolecular Spectroscopy*, 79 (2011) 1605.
41. V. M. Anandakumar, M. A. Khadar, *Cryst. Res. Technol.*, 43 (2008) 193.
42. C. Iwakura, A. Honji, H. Tamura, *Electrochim. Acta*, 26 (1981) 1319.
43. M. H. Mendonca, M. I. Godinho, M. A. Catarino, M. I. da Silva Pereira, F. M. Costa, *Solid State Science*, 4 (2002) 175.
44. M. I. Godinho, M. A. Catarino, M. I. da Silva Pereira, I. H. Mendonca, F. M. Costa, *Electrochim. Acta*, 47 (2002) 4307.
45. R. N. Singh, N. K. Singh, J. P. Singh, G. Balaji, N. S. Gajbhiye, *Int. J. Hydrogen energy*, 31 (2006) 701.
46. M. S. Al-Hosan, J. P. Singh, A. M. Al-Mayouf, A. A. Al-Suhibany, M. N. Shaddad, *Int. J. Electrochem. Sci.*, 7 (2012) 4959.

47. Anindita, A. Singh, R. N. Singh, *Int. J. Hydrogen Energy*, 35 (2010) 3243.
48. R. N. Singh, Madhu, R. Awasthi, A. S. K. Sinha, *J. Solid State Electrochem.*, 13(10) (2009) 1613.
49. R. N. Singh, Madhu, R. Awasthi, A. S. K. Sinha, *Electrochim. Acta*, 54 (2009) 3020.
50. E. Gileadi, *Electrode Kinetics*, (VCH Publishers Inc., New York) 1993, p.151.
51. N. K. Singh, J. P. Singh, R. N. Singh, *Int. J. Hydrogen Energy*, 27 (2002) 895.

© 2020 The Authors. Published by ESG (www.electrochemsci.org). This article is an open access article distributed under the terms and conditions of the Creative Commons Attribution license (<http://creativecommons.org/licenses/by/4.0/>).